Chemical Science

ROYAL SOCIETY OF CHEMISTRY

EDGE ARTICLE

View Article Online
View Journal | View Issue

Cite this: *Chem. Sci.*, 2024, **15**, 511

All publication charges for this article have been paid for by the Royal Society of Chemistry

Received 2nd November 2023
Accepted 4th December 2023

DOI: 10.1039/d3sc05849b

rsc.li/chemical-science

Soluble Gd_6Cu_{24} clusters: effective molecular electrocatalysts for water oxidation†

Jia-Nan Chen,‡ Zhong-Hua Pan,‡ Qi-Hao Qiu, Cheng Wang, La-Sheng Long, Lan-Sun Zheng and Xiang-Jian Kong *

The water oxidation half reaction in water splitting for hydrogen production is extremely rate-limiting. This study reports the synthesis of two heterometallic clusters (Gd_6Cu_{24}-IM and Gd_6Cu_{24}-AC) for application as efficient water oxidation catalysts. Interestingly, the maximum turnover frequency of Gd_6Cu_{24}-IM in an NaAc solution of a weak acid (pH 6) was 319 s^{-1}. The trimetallic catalytic site, H_2O–$Gd^{III}Cu^{II}_2$–H_2O, underwent two consecutive two-electron two-proton coupled transfer processes to form high-valent Gd^{III}–O–O–Cu^{III}_2 intermediates. Furthermore, the O–O bond was formed *via* intramolecular interactions between the Cu^{III} and Gd^{III} centers. The results of this study revealed that synergistic catalytic water oxidation between polymetallic sites can be an effective strategy for regulating O–O bond formation.

Introduction

Hydrogen production by water splitting is a promising solution for future energy needs;[1] however, water oxidation is rate-limiting, primarily due to its four-electron transfer process with slow reaction kinetics.[2] Many researchers have been inspired by natural photosynthesis to develop catalytic systems to resolve this rate-limiting issue.[3] Several studies have developed molecular water oxidation catalysts.[4] In particular, significant efforts have focused on mimicking the structure and catalytic properties of the natural oxygen-evolving complex (OEC), a unique heterometallic-oxide Mn_4CaO_5-cluster, in photosystem II (PS II) of plants, algae, and cyanobacteria.[5] Although several multinuclear clusters simulating OEC structures have been reported,[6] their catalytic performance is still far from that of natural OEC, with the mechanism behind the O–O bond formation still not yet conclusively known.[7] Catalysts usually should easily attain four electrons and contain effective synergistic catalytic structural motifs to achieve a similar catalytic activity.[8] Previous studies on structural motifs have mainly focused on the Mn–O–Mn–H_2O bimetallic structure.[9,10] Recent studies have shown that the redox-inert Ca^{2+} ion in Mn_4CaO_5 may play an important role in maintaining the structural integrity of clusters and supporting ligand sites for water molecules or in assisting proton transfer.[11] However, the poor stability of Ca^{2+}-containing Mn_4CaO_4 clusters in polar solvents has hindered their development.[12] Therefore, developing efficient and stable cluster catalysts for water oxidation remains challenging.

Several studies have recently reported that replacing Ca^{2+} ions with lanthanide ions can stabilize the cluster structure in performance simulations.[6c,13] Furthermore, lanthanide ions have high coordination numbers, rich geometries, and

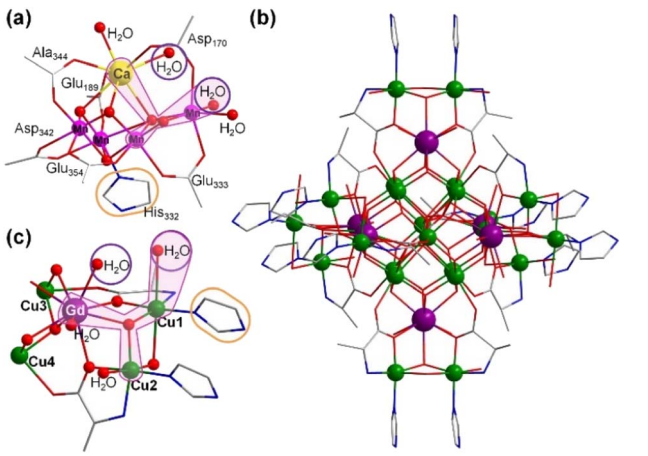

Fig. 1 (a) Structure of the Mn_4CaO_5 cluster. (b) Core of the Gd_6Cu_{24}-IM. (c) Asymmetric unit ($GdCu_4$) of Gd_6Cu_{24}-IM. H_2O–Ca–O–Mn_2–H_2O and H_2O–Gd–O–Cu_2–H_2O motifs are marked in pink and water molecules are marked by a purple circle. Color codes: Gd, purple; Cu, green; Mn, pink; Ca, yellow; C, gray; N, blue; O, red. All H atoms were omitted.

Collaborative Innovation Center of Chemistry for Energy Materials, State Key Laboratory of Physical Chemistry of Solid Surface, Department of Chemistry, College of Chemistry and Chemical Engineering, Xiamen University, Xiamen, 361005, China. E-mail: xjkong@xmu.edu.cn

† Electronic supplementary information (ESI) available: The crystal data and structure of the clusters, experimental details and experimental data. CCDC 2244617 and 2244618. For ESI and crystallographic data in CIF or other electronic format see DOI: https://doi.org/10.1039/d3sc05849b

‡ These authors contributed equally to this work.

structural flexibility.[14] This study reports the synthesis of two high-nuclearity clusters—$[\mathbf{Gd_6Cu_{24}}(IM)_{12}(L\text{-}Al)_{12}(\mu_3\text{-}OH)_{30}(\mu_2\text{-}OH)_6(CO_3)(H_2O)_{24}]\cdot(ClO_4)_{16}\cdot(H_2O)_6$ (**Gd_6Cu_{24}-IM**) and $[\mathbf{Gd_6Cu_{24}}(Ac)_6(L\text{-}Al)_{12}(\mu_3\text{-}OH)_{30}(\mu_2\text{-}OH)_6Cl(H_2O)_{24}]\cdot(ClO_4)_{11}\cdot(H_2O)_{19}$ (**Gd_6Cu_{24}-AC**) (IM = imidazole, L-Al = L-alanine, Ac = acetate)—possessing the same metal core frames (Fig. 1 and S1†). Similar to H_2O–Ca–O–Mn_2–H_2O in OEC, the trimetallic structural motif of H_2O–Gd–O–Cu_2–H_2O in **Gd_6Cu_{24}** may be a potentially efficient synergistic catalytic site for water oxidation.

Results and discussion

Clusters **Gd_6Cu_{24}-IM** and **Gd_6Cu_{24}-AC** were obtained by the reaction of $Gd(ClO_4)_3$, $Cu(ClO_4)_2\cdot 6H_2O$, and L-alanine with imidazole and NaAc, respectively. The asymmetric structural unit $[GdCu_4]$ of **Gd_6Cu_{24}** can be considered as two corner-deficient $[GdCu_2O_3]$ and $[GdCu_2O_4]$ cubes linked together by sharing a Gd^{3+} ion (Fig. 1c). Six $[GdCu_4]$ units were connected by four μ_3-O^{2-}, resulting in an octahedral conformational arrangement. The metal core of **Gd_6Cu_{24}** displayed an octahedral inner core of Gd_6Cu_{12} connected to six outer Cu_2 units. Each $[GdCu_4]$ unit contained five metal ions, in which Gd, Cu_1, and Cu_2 were bound to water molecules. Furthermore, the **Gd_6Cu_{24}-IM** cluster was protected by 12 amino acids and 12 imidazole ligands, highly resembling the peripheral ligands of the OEC. Furthermore, each cluster core unit of **Gd_6Cu_{24}-IM** and **Gd_6Cu_{24}-AC** had 16 and 11 positive charges in addition to 12 sets of water-binding sites, which can promote water oxidation catalysis.

The catalytic properties were characterized in an aqueous solution, and the stability was verified in the high-resolution electrospray ionization mass spectrometry (HRESI-MS) spectra (Fig. S6†). For **Gd_6Cu_{24}-IM**, the peak at 1978.73 can be attributed to $[\mathbf{Gd_6Cu_{24}}(IM)_{12}(L\text{-}Al)_{12}(\mu_3\text{-}OH)_{28}(O)_8(CO_3)_1(H_2O)_{24}(ClO_4)_5]^{3+}$ (Fig. S6a†); for **Gd_6Cu_{24}-AC**, these peaks are observed and can be attributed to $[\mathbf{Gd_6Cu_{24}}(Ac)_x(L\text{-}Al)_{10}(\mu_3\text{-}OH)_{28}(O)_8(H_2O)_2(ClO_4)_{8-x}]^{4+}$ (X = 0–6) (Fig. S6b†). The redox properties of **Gd_6Cu_{24}-IM** and **Gd_6Cu_{24}-AC** were analyzed by cyclic voltammetry (CV) and differential pulse voltammetry (DPV) in an NaAc/HAc buffer solution (0.5 M, pH = 6) (Fig. 2, S7 and S8†). The redox current of **Gd_6Cu_{24}-IM** at $E_{1/2}$ (0.15 V, all potentials were compared to the normal hydrogen electrode, NHE) depended linearly on the square root of the scan rate and corresponded to diffusion control. Moreover, the difference between the cathodic and anodic peak potentials of 30 mV (ΔE_p, Fig. 2a, b and S7†) indicated a two-electron quasi-reversible process.[15] However, the reduction current of **Gd_6Cu_{24}-AC** (Fig. 2c, d and S8†) at 0.13 V was not reversible for the reaction, although it linearly depended on the square root of the scan rate owing to the dissociation of the charged acetate during the reduction process.[16] By performing DPV at a low scan rate, the reduction current corresponded to the splitting of the oxidation current peak into two peaks attributed to two electron transfers as well as the relocation of the acetate ligand. As determining the anodic shoulder peak potential (E_p) of approximately 1.35 V is difficult, the half-peak potential $E_{p/2}$ *versus* ln(ν) was fitted using the Laviron equation (Fig. 3a, b, S9 and S10†).[17] The fitted slope was equal to $RT/(1-\alpha)nF$ for the anodic shoulder peak, where α is the transfer coefficient (0.5) and n was calculated to be 2. These results indicated that the two peripheral Cu^{2+} ions in the $[GdCu_4]$ unit could be considered equivalent groups for the single-electron reaction, *i.e.*, the quasi-reversible process near 0.15 V can be attributed to the reaction pair of two-electron reduction of $\mathbf{Gd_6Cu^{II}_{24}}/Gd_6Cu^{II}_{22}Cu^{I}_{2}$, while the anodic shoulder peak around 1.35 V can be attributed to the two-electron oxidation of $\mathbf{Gd_6Cu^{II}_{24}}/Gd_6Cu^{II}_{22}Cu^{III}_{2}$.[6e]

The DPVs of **Gd_6Cu_{24}-IM** and **Gd_6Cu_{24}-AC** transformed significantly by changing the solvent from superdry acetonitrile

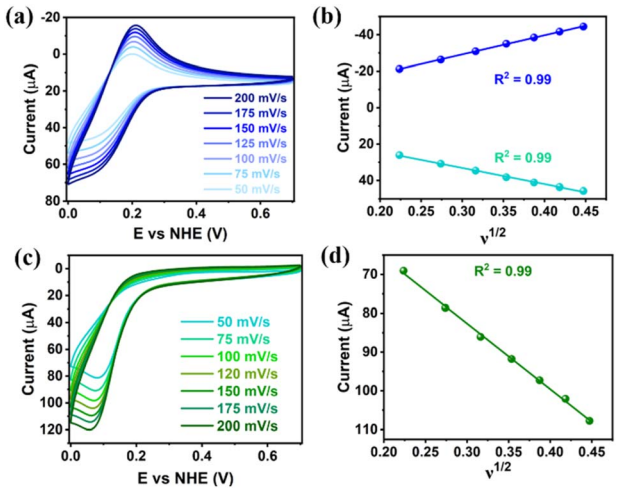

Fig. 2 (a) CV of 0.25 mM **Gd_6Cu_{24}-IM** in 0.5 M NaAc/HAc (pH = 6) buffer solution using a GC electrode with different scan rates (0.05–0.2 V s^{-1}) at 0–0.7 V. (b) Plots of i_p (μA) *vs.* $\nu^{1/2}$ ($V^{1/2}$ $s^{-1/2}$) for **Gd_6Cu_{24}-IM**. (c) CV of 0.25 mM **Gd_6Cu_{24}-AC** in 0.5 M NaAc/HAc (pH = 6) buffer solution using the GC electrode with different scan rates (0.05–0.2 V s^{-1}) at 0–0.7 V. (d) Plots of i_p (μA) *vs.* $\nu^{1/2}$ ($V^{1/2}$ $s^{-1/2}$) for **Gd_6Cu_{24}-AC**.

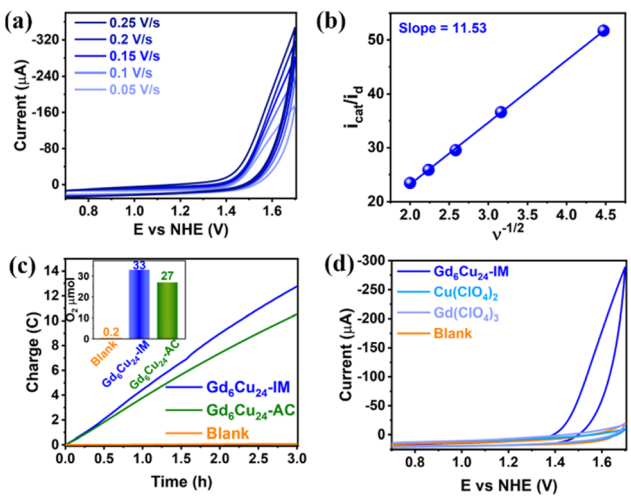

Fig. 3 (a) CVs of **Gd_6Cu_{24}-IM** (0.25 mM) in NaAc/HAc (0.5 M, pH = 6) buffer solution at different scan rates: 50–250 mV s^{-1} at 0.7–1.7 V. (b) Plot of i_{cat}/i_d *versus* $\nu^{-1/2}$ at 1.7 V. (c) CPE data showing charge *versus* time for a 20 mL solution containing NaAc/HAc buffer solution (0.5 M, pH = 6) and 0.25 mM **Gd_6Cu_{24}-IM** and **Gd_6Cu_{24}-AC**. (d) CVs of **Gd_6Cu_{24}-IM** (0.25 mM), $Gd(ClO_4)_3$ (1.5 mM), and $Cu(ClO_4)_2$ (6 mM).

to an aqueous NaAc/HAc buffer solution (pH = 6; Fig. S11 and S12†).[6e,13d] In acetonitrile, the oxidation peak at 1.72 V can be attributed to the two-electron oxidation of the $Gd_6Cu^{II}_{24}/Gd_6Cu^{II}_{22}Cu^{III}_2$ reaction pair. In the NaAc/HAc buffer, the anodic current was significantly enhanced after 1.35 V, thus indicating the occurrence of aqueous oxidation. A linear relationship was observed in the plot of the catalytic peak current *versus* **Gd_6Cu_{24}-IM** concentration (Fig. S13†), thus indicating that the rate law for **Gd_6Cu_{24}-IM** catalyzed water oxidation can be expressed in terms of a pseudo-first-order rate reaction (eqn (1)–(3), ESI†).[18] The catalytic peak currents were directly proportional to the square root of the scan rate, thus indicating a diffusion-controlled catalytic redox process.[19] Linear scan voltammograms (LSV) of **Gd_6Cu_{24}-IM** and **Gd_6Cu_{24}-AC** were recorded on an indium tin oxide (ITO) electrode. The significantly enhanced catalytic currents indicated water oxidation (Fig. S14†). The overpotentials for **Gd_6Cu_{24}-IM** and **Gd_6Cu_{24}-AC** required to reach 1 mA cm^{-2} were 598 and 689 mV, respectively. In comparison to previous reports (Table S2†), the overpotentials represent a relatively lower level. The difference in the overpotentials may be attributed to the different peripheral coordination groups between **Gd_6Cu_{24}-IM** and **Gd_6Cu_{24}-AC** (imidazole and acetate, respectively), and the conjugation effect of imidazole ligands may help to reduce the reaction energy barrier.[20] The apparent rate constants (k_{cat}), called turnover frequency (TOF), for **Gd_6Cu_{24}-IM** and **Gd_6Cu_{24}-AC** at 1.7 V were 319 and 169 s^{-1}, respectively (Fig. 3b and S9†),[21] much higher than those of previously reported mono- and di-nuclear catalysts (0.4–100 s^{-1}).[22]

A gas-tight double-compartment cell with the cathode and anode separated by a Nafion membrane was utilized to verify the release of oxygen. **Gd_6Cu_{24}-IM** (0.25 mM) was subjected to controlled potential electrolysis (CPE) at 1.70 V in an NaAc/HAc buffer solution (0.5 M, pH = 6) using an ITO electrode (1.00 cm^2; Fig. 3c). Electrolysis was performed for 3 h and oxygen production was determined by gas chromatography, where approximately 33 μmol of O_2 were formed with a faradaic efficiency of 94%. The ratio of H_2 to O_2 was measured (2 : 1). For **Gd_6Cu_{24}-IM**, neither the blank nor the inorganic salt catalytic tests showed a significant catalytic current. The reproducibility of the 50 times cycle scan, the almost identical UV-Vis spectra, and the CV curves before and after 3 h of controlled potential electrolysis (Fig. 3d and S15–S18†) indicated that water oxidation occurred under homogeneous catalytic conditions in addition to the high activity and stability of **Gd_6Cu_{24}-IM**.[23]

The DPVs of **Gd_6Cu_{24}** clusters in a mixture of superdry CH_3CN and H_2O at different concentrations were recorded to elucidate the water oxidation mechanism. The results (Fig. 4a) revealed that the DPV curves of **Gd_6Cu_{24}-AC** changed significantly with the addition of water, where the oxidation peak current increased dramatically and the oxidation onset potential shifted positively, indicating that the coordination of water can reduce the oxidation onset potential. The DPV curves of **Gd_6Cu_{24}-IM** changed in a pattern similar to that of **Gd_6Cu_{24}-AC**, although its two oxidation peaks did not show significant splitting (Fig. S19†). Changes in the oxidation onset potential

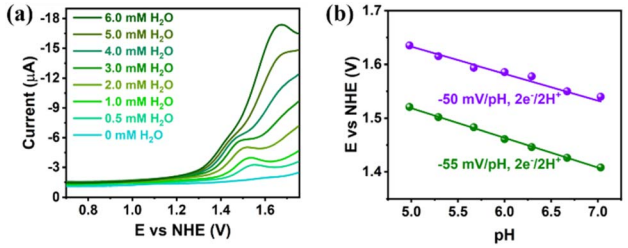

Fig. 4 (a) DPVs of **Gd_6Cu_{24}-AC** (0.25 mM) in CH_3CN with Et_4NClO_4 (0.1 M) before and after addition of different amounts of H_2O. (b) Pourbaix diagram of **Gd_6Cu_{24}-AC** (0.25 mM) in NaAc/HAc (0.5 M, pH 4.98–7.03) buffer solution. E_p values are cited rather than $E_{1/2}$ due to chemical irreversibility.

were observed by changing the pH of the NaAc/HAc buffer solution, indicating that the oxidation process involved a proton-coupled electron transfer (PCET). The Pourbaix diagram revealed that (Fig. 4b) in an NaAc/HAc buffered aqueous solution (0.5 M, pH 4.98–7), two consecutive oxidation peaks of **Gd_6Cu_{24}-AC** exhibited Nernstian responses at approximately −55 and −50 mV pH^{-1}, consistent with the $2e^-/2H^+$ PCET (−59 mV pH^{-1}, Nernstian ideal),[24] while the responses of **Gd_6Cu_{24}-IM** were −54 and −57 mV pH^{-1} (Fig. S22†). In addition, the catalytic processes of **Gd_6Cu_{24}-IM** and **Gd_6Cu_{24}-AC** showed low solvent kinetic isotope effects of 1.23 and 1.25, respectively, ($KIE = k_{H_2O}/k_{D_2O}$, Fig. S23†),[25] significantly different from the hydrophilic nucleophilic attack mechanism of mononuclear catalysts but consistent with the intramolecular O–O bond formation route for Cu_3 catalysts.[26]

Based on the typical mechanisms reported for natural OEC-catalyzed water oxidation,[12b,27] it was inferred that the two molecules of water (W1 and W2) that coordinated on the heterometallic centers Cu^{II} and Gd^{III} can be used as the oxygen source for O–O bond formation (Fig. S24†). W1 and W2 had a distance of 2.81 Å, close to the distance between the two water molecules coordinated on Ca^{II} and Mn^{III} in the OEC (3.26 Å).[28] Based on the experimental results of previous studies and previously reported catalytic mechanisms for water oxidation by multinuclear molecular catalysts,[6e,13d] a plausible and reasonable mechanism for water oxidation catalyzed by **Gd_6Cu_{24}** was proposed (Fig. 5). Under electrolytic catalytic conditions, the trimetallic reaction site is oxidized from the initial $Gd^{III}(OH_2)Cu^{III}_2(OH_2)$ species **1** through a $2e^-/2H^+$ PCET process to give $Gd^{III}(OH)Cu^{III}_2(OH)$ species **2**, which can be further oxidized by the $2e^-/2H^+$ PCET process to $Gd^{III}(O^{\bullet})Cu^{III}_2(O^{\bullet})$ species **3**. The redox potentials of these two steps were 1.35 and 1.55 V, respectively. Species **3** forms species **4**, containing O–O bonds through intramolecular interactions, while species **4** releases O_2 and completes the cycle by coordinating with two water molecules to form starting cluster **1**. The M_3–O_2 intermediate is stabilized by the trimetallic site of $Gd^{III}Cu^{III}_2$, which may facilitate the formation of O–O bonds. This pathway differs from the common mechanism of O–O bond formation by the nucleophilic water attack on the highly oxidized state of M^{n+}=O. The formation of the highly oxidized state of Cu^{IV}=O and ligand hydrocarbon oxidation are also avoided.[29]

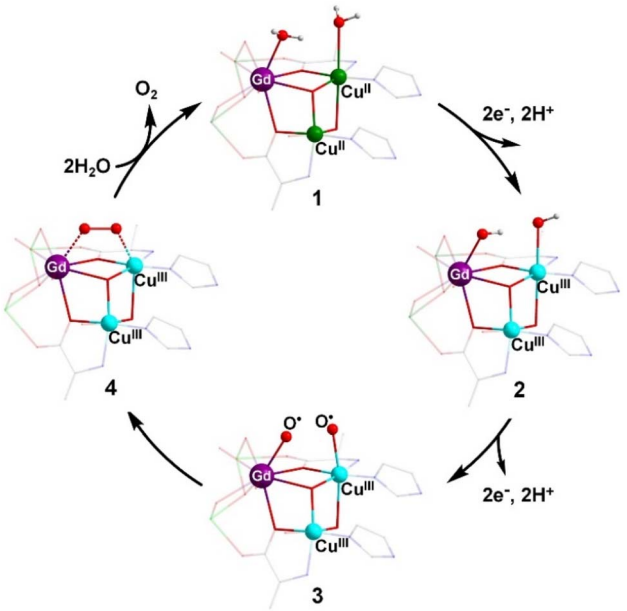

Fig. 5 Proposed catalytic mechanism for the water oxidation based on Gd_6Cu_{24}-IM. Color codes: Gd, purple; Cu^{II}, green; Cu^{III}, turquoise; H, white; C, gray; N, blue; O, red.

Conclusions

In conclusion, this study reported an efficient catalytic water oxidation using water-soluble **Gd_6Cu_{24}** clusters in aqueous solutions of weak acids. The trimetallic catalytic site synergistically catalyzed water oxidation by promoting O–O bond formation, while simple amino acid ligands provided both water solubility and stability, which assisted the catalytic process. Interestingly, the TOFs of **Gd_6Cu_{24}-IM** and **Gd_6Cu_{24}-AC** at 1.7 V reached 319 and 169 s^{-1}, respectively. This work offers a possibility to understand the synergistic effect of multiple metals in the water oxidation mechanism. Furthermore, **Gd_6Cu_{24}** has a tunable molecular structure and metal sites, which is beneficial for designing highly active and stable catalysts in the future.

Data availability

The crystal data and structure of the clusters, experimental details and experimental data for this article are available in the ESI.†

Author contributions

J.-N. C., Z.-H. P. and X.-J. K. conceived and designed the research; J.-N. C. and Z.-H. P. synthesized and characterized the compounds. X.-J. K., J.-N. C., Z.-H. P., Q.-H. Q., C. W., L.-S. L., and L.-S. Z. analyzed the data. J.-N. C., Z.-H. P. and X.-J. K. wrote the manuscript with contributions from all authors. All authors analyzed the data and commented on the manuscript. J.-N. C. and Z.-H. P. contributed equally to this work.

Conflicts of interest

The authors declare no competing financial interest.

Acknowledgements

We gratefully acknowledge the financial support from the National Natural Science Foundation of China (Grant No. 92161104, 92161203, and 21721001).

Notes and references

1 (*a*) T. J. Meyer, *Nature*, 2008, **451**, 778–779; (*b*) A. Cho, *Science*, 2010, **329**, 786–787; (*c*) N. S. Lewis, *Science*, 2016, **351**, aad1920.

2 (*a*) M. D. Kärkäs, O. Verho, E. V. Johnston and B. Åkermark, *Chem. Rev.*, 2014, **114**, 11863–12001; (*b*) X.-P. Zhang, A. Chandra, Y.-M. Lee, R. Cao, K. Ray and W. Nam, *Chem. Soc. Rev.*, 2021, **50**, 4804–4811; (*c*) B. Zhang and L. Sun, *Chem. Soc. Rev.*, 2019, **48**, 2216–2264; (*d*) X.-P. Zhang, H.-Y. Wang, H. Zheng, W. Zhang and R. Cao, *Chin. J. Catal.*, 2021, **42**, 1253–1268.

3 (*a*) N. Nelson and A. Ben-Shem, *Nat. Rev. Mol. Cell Biol.*, 2004, **5**, 971–982; (*b*) Y. Umena, K. Kawakami, J.-R. Shen and N. Kamiya, *Nature*, 2011, **473**, 55–60.

4 (*a*) M. Kondo, H. Tatewaki and S. Masaoka, *Chem. Soc. Rev.*, 2021, **50**, 6790–6831; (*b*) J. Li, C. A. Triana, W. Wan, D. P. A. Saseendran, Y. Zhao, S. E. Balaghi, S. Heidari and G. R. Patzke, *Chem. Soc. Rev.*, 2021, **50**, 2444–2485; (*c*) R. Matheu, P. Garrido-Barros, M. Gil-Sepulcre, M. Z. Ertem, X. Sala, C. Gimbert-Suriñach and A. Llobet, *Nat. Rev. Chem.*, 2019, **3**, 331–341.

5 (*a*) S. Paul, F. Neese and D. A. Pantazis, *Green Chem.*, 2017, **19**, 2309–2325; (*b*) Q.-F. Chen, Y.-H. Guo, Y.-H. Yu and M.-T. Zhang, *Coord. Chem. Rev.*, 2021, **448**, 214164; (*c*) M. Okamura, M. Kondo, R. Kuga, Y. Kurashige, T. Yanai, S. Hayami, V. K. K. Praneeth, M. Yoshida, K. Yoneda, S. Kawata and S. Masaoka, *Nature*, 2016, **530**, 465–468.

6 (*a*) L. Sun, *Science*, 2015, **348**, 635–636; (*b*) B. Gerey, E. Gouré, J. Fortage, J. Pécaut and M.-N. Collomb, *Coord. Chem. Rev.*, 2016, **319**, 1–24; (*c*) R. Yao, Y. Li, Y. Chen, B. Xu, C. Chen and C. Zhang, *J. Am. Chem. Soc.*, 2021, **143**, 17360–17365; (*d*) F. Evangelisti, R. Güttinger, R. Moré, S. Luber and G. R. Patzke, *J. Am. Chem. Soc.*, 2013, **135**, 18734–18737; (*e*) X. Jiang, J. Li, B. Yang, X.-Z. Wei, B.-W. Dong, Y. Kao, M.-Y. Huang, C.-H. Tung and L.-Z. Wu, *Angew. Chem. Int. Ed.*, 2018, **57**, 7850–7854; *Angew. Chem.*, 2018, **130**, 7976–7980; (*f*) C. Chen, Y. Chen, R. Yao, Y. Li and C. Zhang, *Angew. Chem. Int. Ed.*, 2019, **58**, 3939–3942; *Angew. Chem.*, 2019, **131**, 3979–3982; (*g*) W.-S. Gao, J.-M. Wang, N.-N. Shi, C.-N. Chen, Y.-H. Fan and M. Wang, *New J. Chem.*, 2019, **43**, 4640–4647.

7 (*a*) J. Wang, M. Feng, M. N. Akhtar and M.-L. Tong, *Coord. Chem. Rev.*, 2019, **387**, 129–153; (*b*) R. Chen, Z.-H. Yan and X.-J. Kong, *ChemPhotoChem*, 2020, **4**, 157–167.

8 (*a*) M. Gil-Sepulcre and A. Llobet, *Nat. Catal.*, 2022, **5**, 79–82; (*b*) G. Maayan, N. Gluz and G. Christou, *Nat. Catal.*, 2018, **1**, 48–54.

9 (*a*) T. Ghosh and G. Maayan, *Angew. Chem. Int. Ed.*, 2019, **58**, 2785–2790; *Angew. Chem.*, 2019, **131**, 2811–2816; (*b*) A. K. Poulsen, A. Rompel and C. J. McKenzie, *Angew. Chem.*

Int. Ed., 2005, **44**, 6916–6920; *Angew. Chem.*, 2005, **117**, 7076–7080; (*c*) M. D. Kärkäs and B. Åkermark, *Dalton Trans.*, 2016, **45**, 14421–14461.

10 (*a*) X.-J. Su, M. Gao, L. Jiao, R.-Z. Liao, P. E. M. Siegbahn, J.-P. Cheng and M.-T. Zhang, *Angew. Chem. Int. Ed.*, 2015, **54**, 4909–4914; *Angew. Chem.*, 2015, **127**, 4991–4996; (*b*) S. J. Koepke, K. M. Light, P. E. VanNatta, K. M. Wiley and M. T. Kieber-Emmons, *J. Am. Chem. Soc.*, 2017, **139**, 8586–8600; (*c*) Q.-Q. Hu, X.-J. Su and M.-T. Zhang, *Inorg. Chem.*, 2018, **57**, 10481–10484.

11 (*a*) C. F. Yocum, *Coord. Chem. Rev.*, 2008, **252**, 296–305; (*b*) V. Krewald, F. Neese and D. A. Pantazis, *Phys. Chem.*, 2016, **18**, 10739–10750; (*c*) K. Saito, M. Nakagawa, M. Mandal and H. Ishikita, *Photosynth. Res.*, 2021, **148**, 153–159.

12 (*a*) C. Chen, Y. Li, G. Zhao, R. Yao and C. Zhang, *ChemSusChem*, 2017, **10**, 4403–4408; (*b*) Y. Li, R. Yao, Y. Chen, B. Xu, C. Chen and C. Zhang, *Catalysts*, 2020, **10**, 185.

13 (*a*) F. Evangelisti, R. Moré, F. Hodel, S. Luber and G. R. Patzke, *J. Am. Chem. Soc.*, 2015, **137**, 11076–11084; (*b*) D.-F. Lu, X.-J. Kong, T.-B. Lu, L.-S. Long and L.-S. Zheng, *Inorg. Chem.*, 2017, **56**, 1057–1060; (*c*) R. Chen, G.-L. Zhuang, Z.-Y. Wang, Y.-J. Gao, Z. Li, C. Wang, Y. Zhou, M.-H. Du, S. Zeng, L.-S. Long, X.-J. Kong and L.-S. Zheng, *Natl. Sci. Rev.*, 2021, **8**, nwaa234; (*d*) R. Chen, C.-L. Chen, M.-H. Du, X. Wang, C. Wang, L.-S. Long, X.-J. Kong and L.-S. Zheng, *Chem. Commun.*, 2021, **57**, 3611–3614.

14 (*a*) X.-Y. Zheng, X.-J. Kong, Z. Zheng, L.-S. Long and L.-S. Zheng, *Acc. Chem. Res.*, 2018, **51**, 517–525; (*b*) X.-Y. Zheng, J. Xie, X.-J. Kong, L.-S. Long and L.-S. Zheng, *Coord. Chem. Rev.*, 2019, **378**, 222–236; (*c*) Z.-H. Pan, Z.-Z. Weng, X.-J. Kong, L.-S. Long and L.-S. Zheng, *Coord. Chem. Rev.*, 2022, **457**, 214419.

15 P. Ceroni, A. Credi and M. Venturi, in *Analytical Methods in Supramolecular Chemistry*, 2012, pp. 371–457.

16 C. E. Castillo, T. Stoll, M. Sandroni, R. Gueret, J. Fortage, M. Kayanuma, C. Daniel, F. Odobel, A. Deronzier and M.-N. Collomb, *Inorg. Chem.*, 2018, **57**, 11225–11239.

17 E. Laviron, *J. Electroanal. Chem.*, 1979, **101**, 19–28.

18 M. McKinnon and J. Rochford, in *Green Chem.*, ed. B. Török and T. Dransfield, Elsevier, 2018, p. 695–727.

19 Z.-H. Pan, Y.-W. Tao, Q.-F. He, Q.-Y. Wu, L.-P. Cheng, Z.-H. Wei, J.-H. Wu, J.-Q. Lin, D. Sun, Q.-C. Zhang, D. Tian and G.-G. Luo, *Chem.–Eur. J.*, 2018, **24**, 8275–8280.

20 J. S. Pap, Ł. Szyrwiel, D. Srankó, Z. Kerner, B. Setner, Z. Szewczuk and W. Malinka, *Chem. Commun.*, 2015, **51**, 6322–6324.

21 A. M. Geer, C. Musgrave III, C. Webber, R. J. Nielsen, B. A. McKeown, C. Liu, P. P. M. Schleker, P. Jakes, X. Jia, D. A. Dickie, J. Granwehr, S. Zhang, C. W. Machan, W. A. Goddard III and T. B. Gunnoe, *ACS Catal.*, 2021, **11**, 7223–7240.

22 (*a*) S. M. Barnett, K. I. Goldberg and J. M. Mayer, *Nat. Chem.*, 2012, **4**, 498–502; (*b*) M. K. Coggins, M.-T. Zhang, Z. Chen, N. Song and T. J. Meyer, *Angew. Chem. Int. Ed.*, 2014, **53**, 12226–12230; *Angew. Chem.*, 2014, **126**, 12422–12426; (*c*) H. Kuilya, N. Alam, D. Sarma, D. Choudhury and A. Kalita, *Chem. Commun.*, 2019, **55**, 5483–5486; (*d*) K. J. Fisher, K. L. Materna, B. Q. Mercado, R. H. Crabtree and G. W. Brudvig, *ACS Catal.*, 2017, **7**, 3384–3387; (*e*) P. Garrido-Barros, D. Moonshiram, M. Gil-Sepulcre, P. Pelosin, C. Gimbert-Suriñach, J. Benet-Buchholz and A. Llobet, *J. Am. Chem. Soc.*, 2020, **142**, 17434–17446; (*f*) L.-L. Zhou, T. Fang, J.-P. Cao, Z.-H. Zhu, X.-T. Su and S.-Z. Zhan, *J. Power Sources*, 2015, **273**, 298–304.

23 K. J. Lee, B. D. McCarthy and J. L. Dempsey, *Chem. Soc. Rev.*, 2019, **48**, 2927–2945.

24 M. Schulze, V. Kunz, P. D. Frischmann and F. Würthner, *Nat. Chem.*, 2016, **8**, 576–583.

25 S. J. Edwards, A. V. Soudackov and S. Hammes-Schiffer, *J. Phys. Chem. A*, 2009, **113**, 2117–2126.

26 Q.-F. Chen, Z.-Y. Cheng, R.-Z. Liao and M.-T. Zhang, *J. Am. Chem. Soc.*, 2021, **143**, 19761–19768.

27 (*a*) J. Barber, *Nat. Plants*, 2017, **3**, 17041; (*b*) K. Kawashima, T. Takaoka, H. Kimura, K. Saito and H. Ishikita, *Nat. Commun.*, 2018, **9**, 1247; (*c*) P. E. M. Siegbahn, *Biochim. Biophys. Acta, Bioenerg.*, 2013, **1827**, 1003–1019; (*d*) B. Zhang and L. Sun, *ChemSusChem*, 2019, **12**, 3401–3404.

28 M. Suga, F. Akita, K. Hirata, G. Ueno, H. Murakami, Y. Nakajima, T. Shimizu, K. Yamashita, M. Yamamoto, H. Ago and J.-R. Shen, *Nature*, 2015, **517**, 99–103.

29 A. Conde, L. Vilella, D. Balcells, M. M. Díaz-Requejo, A. Lledós and P. J. Pérez, *J. Am. Chem. Soc.*, 2013, **135**, 3887–3896.